

Development of higher-order model for nonlinear interactions in hyperspectral data of mangrove forests

Somdatta Chakravorty^{1,*} and Devadatta Sinha²

¹Department of Information Technology, Government College of Engineering and Ceramic Technology, Kolkata 700 010, India

²Department of Computer Science and Engineering, Calcutta University, Kolkata 700 098, India

The present article analyses the accuracy of application of higher-order nonlinear interaction models on hyperspectral data to identify mangrove mixtures present in the Sunderbans Delta – a World Heritage Site in West Bengal, India. It is observed that intra-species interaction between similar mangrove species (interaction between the same type of end-members) in a homogeneous mangrove stand is more accurately modelled by the linear–quadratic model and hence results in more accurate fractional abundance estimations after unmixing when compared with linear–unmixing models. Specifically, we observe that quadratic models provide more accurate estimates than linear and bilinear models for the study area (Henry Island of Sunderbans), which is mostly dominated by pure and mixed mangrove species of *Avicennia marina*, *Excoecaria agallocha*, *Avicennia alba*, *Phoenix paludosa*, *Avicennia officinalis*, *Ceriops decandra*, *Bruguiera cylindrica* and *Aegialitis*. In this study, the quadratic nonlinear model successfully characterizes the interaction of end-member mixtures comprising *E. agallocha*, *A. officinalis*, *B. cylindrica* and *A. alba* in the study area.

Keywords: Higher-order interaction models, hyperspectral data, mangrove species, nonlinear interactions.

HYPERSPECTRAL remote sensing (HSRS) is a powerful tool for detailed spatio-temporal mapping and sustainable management of large forested lands. The wide spectral range of hyperspectral data and their high spectral resolution allows for accurate detection and classification of surface canopies and ground features through the application of hyperspectral image processing algorithms^{1,2}. For example, the characteristic bio-optical properties of different mangrove species in a dense mangrove forest can be integrated into spectral libraries for improved discrimination and mapping of mangrove eco-types.

Outside India, researchers have made a detailed study of mangroves at species level using hyperspectral data^{3–5}. Studies in India have also established the capability of hyperspectral data for species-level discrimination of mangroves in distantly located islands of the Sunderban

Delta. The Delta is well-known for its homogeneous and heterogeneous patches of mangrove species that include a particular form or various forms of mangrove species within the ecosystem. Application of remote sensing technologies for accurate identification and discrimination of mangrove species is being considerably encouraged in recent times. Homogeneous mangrove areas could be identified through linear spectral unmixing, which follows the principle of singular reflection with negligible multiple scattering⁶. However, in natural forests such as the Sunderban Biosphere Reserve, intra- and inter-species scattering occurs, thus making the reflections nonlinear in nature⁷. Nonlinear spectral unmixing is expected to provide a more accurate estimate of fractional abundance estimation of mangrove mixtures along with their identification.

Nonlinear models have been developed at microscopic scale for materials which are intimately mixed⁸. Such mixtures have been observed and studied for imaged scenes composed of sand or mineral mixtures. Based on ray tracing theory, several hypotheses have been derived to precisely illustrate the relationship between radiation interactions of surfaces comprising microscopic particles. Another type of nonlinear interaction occurring at macroscopic scale has also been studied, particularly in multilayered configurations. Such interactions normally take place when the radiation reflected by an object hits an adjacent object and suffers further reflections before being finally intercepted by the sensor. These cases are common for images acquired over forests where there are multiple reflections between adjacent objects. This is often the case for scenes acquired over forested areas, where there may be many interactions between the ground and the canopy. The models of Fan *et al.*⁹ and Nascimento and Bioucas-Dias¹⁰ have been developed to analytically describe these interactions. They are usually considered for second-order interactions; orders greater than two are neglected. However, in natural forests such as the Sunderban mixed mangrove forest, there exist mixtures of mangrove species with more than two species within a pixel area. Hence, we have developed a nonlinear model considering higher-order interactions between different end-members up to the order of n to

*For correspondence. (e-mail: csomdatta@rediffmail.com)

overcome the limitations of the previous models. Moreover, all these interaction models only include inter-component interactions, but no intra-component interactions. As the target end-members in the study area may occur in pure patches, multiple scattering between similar end-members should not be ignored. Hence, our model also includes interaction terms of similar end-members to get a more accurate representation of abundance values and their contribution to the final reflectance.

Nonlinear mixture models developed till date suggest that if linear spectral unmixing is applied to a nonlinear system, the error in fractional abundance estimates for mineral congregations may be about 30% (ref. 11). In studies regarding vegetation landscapes also, the effect of nonlinearity has been reported^{12–15}. Nonlinear models have been applied on AVIRIS imagery of surfaces comprising mineral ensembles. Roberts *et al.*¹⁴ estimated end-member fractional abundances from nonlinear mixtures of vegetation and canopy shade. Guilefoyle *et al.*¹⁶ and Plaza *et al.*¹⁷ designed neural networks for spectral unmixing of pixel mixtures. The quality of training data for neural networks is responsible for their performance to a great extent. Nonlinear algorithms derived from linear ones have also been used for develop kernel-based nonlinear models^{18–20}. In this case kernels have been applied to the spectral profile of each end-member, independent of radiation interactions between objects, consequently working as nonlinear distortion functions. Other studies on nonlinear unmixing include polynomial post-nonlinear mixing model^{21,22}, nonlinear spectral unmixing for abundance estimates of tree cover in orchards²³, unmixing based on a nonlinear fluctuation model²⁴ and enhancement of unmixing with spatial correlations²⁵.

The major goal of this study is to extract hyperspectral data for mangrove species discrimination with use of higher-order nonlinear interaction models. This higher-order representation considers radiation interaction between different mangrove species (end-members) located in close proximity, which has been overlooked in linear mixing models. An effort has been made to apply this theory in the natural state of the mangrove forests of the Sunderban and perceive how best it can explain the resulting spectra for specific mixed end-member distributions. Pure end-members in the diverse mangrove forest of the Sunderban largely comprise of mangrove species like *Avicennia officinalis*, *Phoenix paludosa*, *Avicennia marina*, *Avicennia alba*, *Bruguiera cylindrica*, etc.

It is of significance to mention that the application of linear–quadratic model for identification of mangrove species is an unexplored field of research.

Study area

The mangrove habitats of Henry island (Figure 1), extending from 21°36'00"N to 21°34'00"N lat. and

86°16'30"E to 88°18'30"E long. of the Sunderban Bio-Geographic Province, West Bengal, India, have been chosen for the present study. The Island is spread out over an area covering 10 sq. km. Henry Island offers a perfect location of hyperspectral remote sensing for mangrove species monitoring and mapping.

A broad depiction of mangrove distribution in Henry Island is that *Excoecaria agallocha*, *A. marina* and *A. alba* dominate the seaward face. Following this precinct is a zone of mixed mangroves comprising *A. officinalis*, *Phoenix paludosa*, *Bruguiera cylindrica*, *Ceriops*, *Xylocarpus*, *Aegialitis* and *E. agallocha*.

Methodology

Data collection

The Hyperion image of Henry Island has been procured from the United States Geological Survey, EROS Center through Data Request and was acquired on 27 May 2011. The acquired imagery has a spatial resolution of 30 m and a wide spectral range from 355 to 2577 nm with a narrow bandwidth of 10 nm.

Data preprocessing

Atmospheric correction has been done on the Hyperion data using FLAASH and QUAC algorithm available in the image processing software, ENVI²¹. FLAASH has been found to be highly proficient for atmospheric correction of data captured by the Hyperion sensor. Execution of FLAASH algorithm exhibits improved correction results in comparison to QUAC, as it considers information of the atmospheric setting of Henry Island at the time of attainment of data. QUAC does not consider the environmental conditions as in FLAASH. Figure 2 *a–c* shows



Figure 1. Satellite image of Henry Island, Sunderban, India (courtesy: Google Earth).

the spectral profile of a mangrove patch before and after executing FLAASH and QUAC. The visible segment of the electromagnetic spectrum in the FLAASH-corrected spectral profile shows that the chlorophyll pigments in flora strongly reflect the green wavelength and absorb blue and red, displaying a typical reflectance crest inside the green range (which is a representative vegetation signature). However, after QUAC correction the rise in reflectance in the green wavelength is not so prominent.

Topographic sheets of Henry Island have been used for precise geo-registration of the Hyperion image²⁶. The SOI Mapsheet No. 79C6SW and 79C6NW has been used for geo-registration. Dimensionality reduction of the hyperspectral bands has been done using Minimum Noise Fraction (MNF) algorithm, which adequately retains the vital data for successful spectral unmixing in the lower dimension.

Ground survey

A ground assessment of the area under study has been made to recognize and gather samples of mangrove

species whose image-based categorization has been carried out. Field visit for initial ground truthing was made in the month of June 2011 immediately after acquisition of data. GPS (accuracy 4 m) was used to accurately position the geographical coordinates of the study track. In the initial visit for ground truthing, a quadrat of 30 m × 30 m dimension that is equal to the spatial resolution of Hyperion imagery was chosen to estimate the presence of dominant mangrove species on the ground. Thirty sample plots were recognized in homogeneous and mixed patches of mangrove species and plotted on the geometrically corrected hyperspectral data with the help of GPS²⁷. A pure or mixed patch was considered depending on the size of a mangrove tree crown or canopy. The number of trees of different species present within the quadrat was counted. The quadrat with tree species having more than 50% presence and selected as the dominant species in that location, represented a homogeneous stand of the mangrove species. The quadrat in which none of the mangrove species had 50% presence was considered as a mixed mangrove patch. These coordinates served as checkpoints to assess precision among image-derived and field-located values of the mangrove species. Ground survey for validation of unmixing results was again done in May 2012 and June 2013. It was observed that the changes in physical abundance of trees within a span of 1–2 years in the island are negligible. Table 1 displays some geographic coordinates of the study area that have been considered as sample plots.

Automated end-member detection

End-member detection is the task of identifying and extracting spectrally pure pixels present in the image scene. The NFINDER (N Finder, where N stands for the number of end-members) algorithm, a well-known technique of end-member identification has been used for extraction of pure mangrove spectra dataset^{28–30}. The algorithm requires some familiarity of the number of dominant end-members that are likely to exist in the study area and searches for the set of input pixels that result in the maximum volume.

Nonlinear model

The Sunderban Biosphere Reserve is characterized by both ‘homogeneous’ and ‘mixed’ mangrove species patches that comprise a particular or several types of mangrove species in a closed ecosystem. Appropriate recognition and categorization of such homogeneous and mixed mangrove patches using various technologies of remote sensing is being encouraged throughout the globe. Detection of mangrove species existing in homogeneous patches might be achieved through linear spectral unmixing⁶. A linear model assumes singular reflection from the target

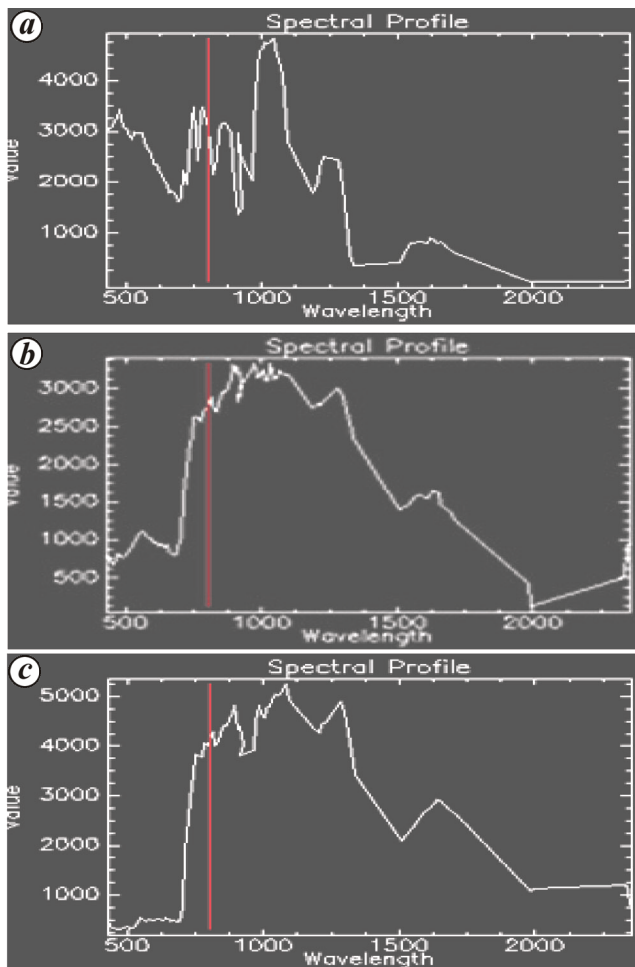


Figure 2. Spectral profile of mangrove forest area: *a*, original data; *b*, after FLAASH correction; *c*, after QUAC correction.

Table 1. Sample quadrats during ground survey

Geographic coordinates	Mangrove species identified	Percentage of mangrove trees in the quadrat	Type of cover (pure/mixed)
21°34.621'; 88°16.502'	<i>Excoecaria agallocha</i>	100	Pure
21°34.626'; 88°16.499'	<i>Avecennia officinalis</i>	100	Pure
21°34.630'; 88°16.490'	<i>A. officinalis</i>	100	Pure
21°34.616'; 88°16.512'	<i>E. agallocha</i>	17	Mixed
	<i>A. officinalis</i>	74	
	<i>Avicennia alba</i>	9	
21°34.650'; 88°16.788'	<i>Avicennia marina</i>	100	Pure
21°34.642'; 88°16.799'	<i>A. marina</i>	100	Pure
21°34.631'; 88°16.810'	<i>A. marina</i>	100	Pure
21°34.621'; 88°16.823'	<i>A. marina</i>	100	Pure
21°34.380'; 88°17.807'	<i>Ceriops decandra</i>	65	Mixed
	<i>E. agallocha</i>	35	
21°34.385'; 88°17.811'	<i>C. decandra</i>	70	Mixed
	<i>E. agallocha</i>	30	
21°34.374'; 88°16.810'	<i>Ceriops tagal</i>	60	Mixed
	<i>E. agallocha</i>	40	
21°34.374'; 88°16.812'	<i>C. tagal</i>	70	Mixed
	<i>E. agallocha</i>	30	

end-member and negligible interaction between its surrounding end-members. In linear spectral unmixing, assuming y as the intensity value of each pixel in the hyperion image and m_r as the matrix representing the signature of pure mangrove species identified by NFINDR, the fractional abundance a_r is estimated using the equation

$$y = \sum_{r=1}^R a_r m_r,$$

However, in mixed natural forests like the Sunderban nonlinear models that consider radiation interaction between several objects within a pixel area and manifold scattering between the plant canopies are likely to provide precise end-member detection of species and their abundance estimation.

In bilinear models, it is implicit that the radiation incident on each mangrove end-member suffers reflections with other mangrove species existing in close vicinity³¹. The radiation reflected from the initial end-member is reflected once more by the subsequent end-member and then intercepted by the satellite sensor. This is known as second-order interaction amongst mangrove species end-members. Thus, for R different end-members, it should have $R*(R + 1)/2$ reflections. The nonlinear reflection model is given below

$$y = \sum_{r=1}^R a_r m_r + \sum_{i=1}^{R-1} \sum_{j=i+1}^R \beta_{i,j} m_i \odot m_j + n. \tag{1}$$

Here y is the intensity value of each pixel in the image, m_r a matrix representing the signature of pure mangrove species identified by NFINDR and a_r , is the estimated fractional abundance of the identified end-members and their mixtures. In this model, reflections of orders larger than two are ignored. Nevertheless, in naturally occurring forests such as the Sunderban Delta, there exist mixtures of mangrove species with more than two species co-existing within a pixel area. We have developed a nonlinear unmixing algorithm for considering higher-order reflections involving dissimilar end-members up to the order of n and observed how well they portray the mixed spectral signatures for specific end-member distributions. The model also includes interaction terms between similar end-members to get a more accurate representation of fractional abundances in the pixel reflectance values.

Unmixing model

Intra-species interaction model: The target end-members in the study area may occur in pure patches covering the entire pixel area or in mixed proportions. In such a situation, multiple scattering between similar end-members should not be ignored. In such cases, application of linear or bilinear model would lead to inaccurate results. Hence, it becomes essential to include interaction terms of similar end-members besides different end-members to get a more accurate representation of abundance values and their contribution to the final reflectance. The algorithm in this model considers intra-end-member interaction of the second-order.

The total number of interactions in this model has been calculated as

$$(R + R + {}^R C_2) = R + R + ((R*(R - 1))/2) = (R*(R + 3)/2).$$

The model is represented by the equation

$$Y = \sum a_r m_r + \sum_{i=1}^R \sum_{j=1}^R \beta_{i,j} m_i * m_j + n. \tag{2}$$

Inter-species interaction model of higher-order: Earlier studies indicate that nonlinear models have considered only bilinear interactions. However, it is observed that in natural forests such as the Sunderban Biosphere Reserve, the mangrove species mostly coexist in mixed form, i.e. a pixel may contain more than two types of end members. In this article we have considered a model with n number of variables representing higher-order interaction of n th order between mangrove species end-members.

The total number of interactions of the third-order in this model has been calculated as

$$\begin{aligned} &= (R + R + {}^R C_2 + {}^R C_3) = R + R + \{[R*(R - 1)]/2\} \\ &+ \{[R*(R - 1)*(R - 2)]/6\} = \{R*(R + 3)/2\} \\ &+ \{[R*(R - 1)*(R - 2)]/6\} \\ &= \{[(3*R*R + 3)] + [R*(R - 1)*(R - 2)]\}/6. \end{aligned}$$

The model extends the linear and bilinear interaction as above with third-order interaction terms as

$$\begin{aligned} Y &= \sum a_r m_r + \sum_{i=1}^R \sum_{j=1}^R \beta_{i,j} m_i * m_j \\ &+ \sum_{i=1}^{R-2} \sum_{j=i+1}^{R-1} \sum_{k=j+1}^R \beta_{i,j,k} (m_i * m_j, m_k) + n_g. \end{aligned} \tag{3}$$

Here $(m_i * m_j * m_k)$ denotes the Hadamard product, i.e. term-by-term multiplication of the i th, j th and k th end-member spectra.

Nth order interaction: The N th order interaction model can be defined as

$$\begin{aligned} Y &= \sum a_r m_r + \sum_{i=1}^R \sum_{j=1}^R \beta_{i,j} m_i * m_j \\ &+ \sum_{i=1}^{r-(n-1)} \sum_{j=(i+1)}^{r-(n-2)} \sum_{k_1=(j+1)}^{r-(n-3)} \dots \sum_{k_n=(k_{(n-1)+1})}^r i, j, k_1, \dots, k_n \\ &\times (m_i * m_j * m_{k_1} * \dots * m_{k_n}) + n_g, \end{aligned} \tag{4}$$

where n_g is the noise and n is the number of interactions.

Accuracy assessment

To authenticate the results estimated using the linear and nonlinear higher-order models, the fractional abundances of the recognized mangrove species have been calculated. The absolute error in the estimated abundance values of every end-member is the absolute difference between the fraction abundance values obtained by the linear or nonlinear higher-order models and that by the real ground information of a particular pixel coordinate. The root mean square error (RMSE) has been estimated as

$$RMSE = 1/NR \sum_{k=1}^N |f_{ck} - f_{mk}|^2,$$

where f_{ck} is the real ground information fraction results, and f_{mk} is the linear/nonlinear model abundance output, N the number of mangrove end-members and R is the number of pixel coordinates whose error values are to be calculated.

Results and analysis

The NFINDR extracted end-members have been taken as input for execution of linear and nonlinear algorithms. With seven principal mangrove species recognized, we have assumed that mixed mangrove species consist of a blend of single and additional variety of these species. The execution of bilinear model (second-order) has resulted in 28 outcomes (seven single (linear) interactions of the end-member and 21 inter-species interactions amongst different end-members). Consideration of intra-end-member interaction in a bilinear model has led to the linear-quadratic model that results in 35 interactions (7 linear reflections, 7 intra-end-member interactions and 21 inter-end-member interactions). The pixel areas that have three end-member mixtures follow the model with third-order interactions and consider a total of 70 interactions (7 linear reflections, 7 intra-end-member interactions, 21 inter-end-member interactions of the second-order and 35 inter-end-member interactions of third-order). Depending upon the type of end-members present within a pixel area, an N th-order nonlinear model (eq. (4)) has been developed. If the pixel is pure, then the model is reduced to an intra-species interaction model (eq. (2)). If the pixel is a two-species mixture, then it reduces to a bilinear model (eq. (1)), and if it is a three-species mixture, the model reduces to eq. (3). Table 2 shows the abundance estimates and RMSE values of an *A. alba*-*A. officinalis*-*E. agallocha*-*B. cylindrica* mixed mangrove patch.

It is observed that the fourth-order and then the third-order models are most accurate for 3-4 mangrove species mixture. As the linear model does not consider mixture

Table 2. Abundance estimates and RMSE values of *E. agallocha*–*A. officinalis*–*B. cylindrica*–*A. alba* patch

End-members	Linear model	Bilinear model	Linear–quadratic model	Model of third-order interaction	Model of fourth-order interaction	Ground truth
1 <i>E. agallocha</i>	0.5833	0.3710	0.2412	0.2274	0.2264	0.24
4 <i>A. alba</i>	0.1009	0.0587	0.0369	0.0406	0.0404	0.04
6 <i>B. cylindrica</i>	0.1110	0.0657	0.0499	0.0469	0.0467	0.05
7 <i>A. officinalis</i>	0.2048	0.1299	0.0810	0.0804	0.0800	0.08
1, 1	–	–	0.2916	0.2604	0.2592	0.24
1, 4	–	0.0713	0.0446	0.0465	0.0463	0.05
1, 6	–	0.0799	0.0603	0.0537	0.0534	0.05
1, 7	–	0.1579	0.0979	0.0920	0.0916	0.09
4, 4	–	–	0.0068	0.0083	0.0083	0.01
4, 6	–	0.0126	0.0092	0.0096	0.0095	0.01
4, 7	–	0.0250	0.0150	0.0164	0.0164	0.02
6, 6	–	–	0.0125	0.0111	0.0110	0.02
6, 7	–	0.0280	0.0202	0.0190	0.0189	0.02
7, 7	–	–	0.0329	0.0325	0.0324	0.03
1, 4, 6	–	–	–	0.0110	0.0109	0.01
1, 4, 7	–	–	–	0.0188	0.0187	0.02
1, 6, 7	–	–	–	0.0217	0.0216	0.03
4, 6, 7	–	–	–	0.0039	0.0039	0.01
1, 4, 6, 7	–	–	–	–	0.0044	0.005
RMSE	0.2315	0.0761	0.0398	0.0211	0.0188	

Table 3. Abundance estimate and RMSE values of *E. agallocha* pure patch

Coordinate (96, 126): End members	Linear spectral unmixing	Linear–quadratic mixing model (LQM)	Ground truth
1	1.000	0.5000	0.5
1, 1		0.5000	0.5
RMSE	0.2673	0.1109	

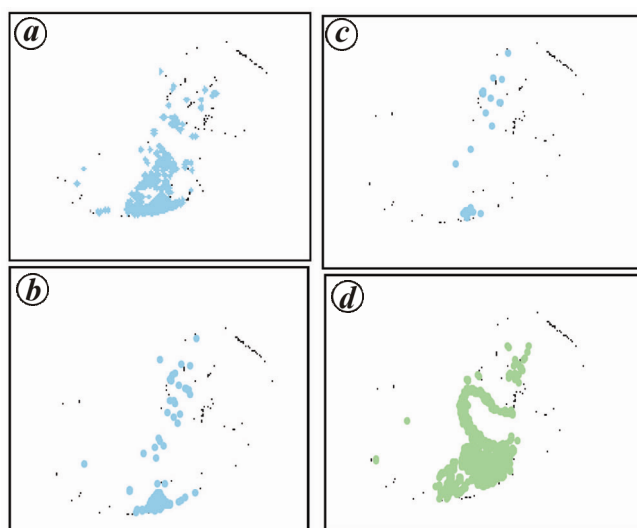


Figure 3. Abundance of *Avicennia alba*: *a*, Linear model; *b*, Bilinear model; *c*, Linear–quadratic model (pixels showing 40% abundance and above). *d*, Abundance of *A. alba*–*Excoecaria agallocha*–*Bruguiera cylindrica* mixture (pixels showing abundance values of 1% and above).

interactions at all, it shows least accuracy. The bilinear model considers only two end-member mixture interactions; hence, it shows lower accuracy compared to the third- and fourth-order models. The abundance estimated

for four-species interactions is very low, which indicates that the mixture presence of the four species is almost negligible, though there is presence of individual end-members to an extent. Figure 3 *a–d* shows a comparison of fractional abundance images generated with the four models for *E. agallocha* and *A. alba* patch and their interactions for the above coordinates.

Table 3 shows the abundance estimate and RMSE value of *E. agallocha* pure patch. The linear–quadratic model shows higher accuracy than the linear model, as it considers interaction between similar species which the linear model does not. The pixel value of a 30 m × 30 m pure mangrove species patch represents the reflectance of that particular mangrove species. When linear interactions are considered, the final pixel value is a representation of single scattering of radiation from the target species to the sensor. This model gives accurate results if the trees are set side by side as in a checkerboard. In such cases, the final reflectance value of a pixel represents single reflection (radiation falling on a tree and getting reflected back and intercepted by the sensor). However, in pure and dense mangrove patches, the same type of mangrove species occur close to each other and hence encounter multiple bounces of reflection between the closely spaced trees. In these cases, the final pixel value is a combination of single and multi-level reflections. As

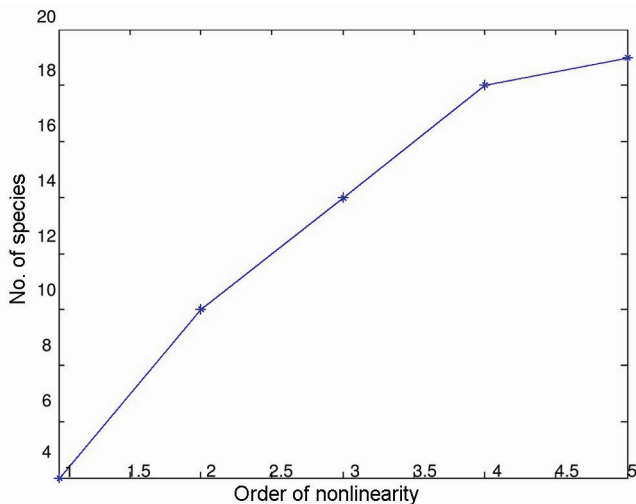


Figure 4. Number of identified mangrove species (pure and mixed) versus order of non-linearity.

our intra-species interaction model considers linear as well as multiple-level reflections, it gives more accurate fractional abundance information for pixels representing a pure mangrove patch than a linear model (Table 3).

Figure 4 displays the increase in the number of identified mangrove species (pure and mixed) with increase in the order of nonlinearity. Though higher-order models result in more accurate identification of end-members and fractional abundance estimation, they have some limitations. The increase in order leads to an increase in computational complexity and processing time. However, in the study of mangrove species identification and their mixtures, possibility of the presence of more than four species within a hyperspectral pixel area is almost negligible. Hence for mangrove forests in particular, computational complexity up to fourth-order is manageable. For higher number of end-members we may separate linearly separable end-members before we apply nonlinear models on them.

Conclusion

This study analyses the precision of applying the nonlinear higher-order interaction model on mangrove species mixtures in the Henry Island of the Sunderban Delta. With the goal of class separation of mangrove species in a mixed mangrove forest, the fractional abundance values of the mangrove end-members and their mixed composition in each pixel area have been calculated using the above stated models. The models developed for similar end-member interactions and N th-order interactions have been analysed and compared with the existing linear and bilinear models in terms of performance accuracy to recognize mixed mangrove species within a pixel. It has been found that in mixed natural mangrove forests, higher-

order nonlinear models are more appropriate than linear mixing models. Linear models are known to be more suitable for detection of end-members that are set in distinct and isolated patches and have given accurate results in areas of pure mangrove. From the results it has also been observed that the similar end-member interaction models are better suited for interactions between similar species in a pure patch and hence give more accurate abundance estimates for pure patches when compared with linear spectral unmixing models. The higher-order nonlinear model has effectively recognized the interfaces among two or more dissimilar end-members in mixed mangrove areas. The study area is found to be dominated by *E. agallocha*, *A. marina* and *A. alba*. Other predominant mangrove species recognized from the hyperspectral image scene are *A. officinalis*, *P. paludosa*, *C. decandra* and *B. cylindrica* along with their mixtures.

1. Bioucas-Dias, J. M., Plaza, A., Dobigeon, N., Parente, M., Du, Q., Gader, P. and Chanussot, J., Hyperspectral unmixing overview: geometrical, statistical, and sparse regression-based approaches. *IEEE J. Sel. Top. Appl. Earth Obs. Remote Sensing*, 2012, **5**(2), 354–379.
2. Demuro, M. and Chisholm, L., Assessment of hyperion for characterizing mangrove communities. In Proceedings of the International Conference AVIRIS Workshop, Pasadena, CA, USA, 2003, pp. 18–23.
3. Vaiphasa, C., Innovative genetic algorithm for hyperspectral image classification. In Proceedings of the International Conference MAP ASIA, Kuala Lumpur, Malaysia, 2003; <http://www.gisdevelopment.net/technology/ip/ma03071abs.htm>
4. Vaiphasa, C. and Ongsomwang, S., Hyperspectral data for tropical mangrove species discrimination. In Proceedings of the 25th Asian Conference on Remote Sensing, Chiang Mai, Thailand, 2004, pp. 22–28.
5. Vaiphasa, C. and Ongsomwang, S., Tropical mangrove species discrimination using hyperspectral data: a laboratory study. *Estuarine Coastal Shelf Sci.*, 2005, **65**(1–2), 371–379.
6. Keshava, N. and Mustard, J. F., Spectral unmixing. *IEEE Signal Process. Mag.*, 2002, **19**(1), 44–57.
7. Johnson, P. E., Smith, M. O., Taylor-George, S. and Adams, J. B., A semi-empirical method for analysis of the reflectance spectra of binary mineral mixtures. *J. Geophys.*, 1983, **88**, 3557–3561.
8. Hapke, B., *Theory of Reflectance and Emittance Spectroscopy*, Cambridge University Press, Cambridge, UK, 1993.
9. Fan, W., Hu, B., Miller, J. and Li, M., Comparative study between a new nonlinear model and common linear model for analysing laboratory simulated-forest hyperspectral data. *Int. J. Remote Sensing*, 2009, **30**(11), 2951–2962.
10. Nascimento, J. M. P. and Bioucas-Dias, J. M., Nonlinear mixture model for hyperspectral unmixing. In Proceedings of the SPIE Image and Signal Processing for Remote Sensing XV (eds Bruzzone, L., Notarnicola, C. and Posa, F.), Berlin, Germany, 2012, 7477.
11. Mustard, J. F. and Sunshine, J. M., Spectral analysis for earth science: investigations using remote sensing data. In *Remote Sensing for the Earth Sciences*, Wiley, New York, 1999, pp. 509–564.
12. Huete, A. R., Jackson, R. D. and Post, D. F., Spectral response of a plant canopy with different soil backgrounds. *Remote Sensing Environ.*, 1985, **17**, 37–53.
13. Smith, M. O., Ustin, S. L., Adams, J. B. and Gillespie, A. R., Vegetation in deserts: a regional measure of abundance from multispectral images. *Remote Sensing Environ.*, 1990, **31**, 1–26.

RESEARCH ARTICLES

14. Roberts, D. A., Smith, M. O. and Adams, J. B., Green vegetation, non-photosynthetic vegetation, and soils in AVIRIS data. *Remote Sensing Environ.*, 1993, **44**, 117–126.
15. Boardman, J., Kruse, F. and Green, R., Mapping target signatures via partial unmixing of AVIRIS data. In Summaries of the 5th Annual JPL Airborne Geoscience Workshop (ed. Green, R.), Pasadena, CA, JPL Publ, 1995, vol. 1, pp. 23–26.
16. Guilfoyle, K. J., Althouse, M. L. and Chang, C.-I., A quantitative and comparative analysis of linear and nonlinear spectral mixture models using radial basis function neural networks. *IEEE Geosci. Remote Sensing Lett.*, 2001, **39**(8), 2314–2318.
17. Plaza, J., Martínez, P., Pérez, R. and Plaza, A., Nonlinear neural network mixture models for fractional abundance estimation in AVIRIS hyperspectral images. In Proceedings of the NASA Jet Propulsion Laboratory AVIRIS Airborne. Earth Science Workshop, Pasadena, CA, 2004.
18. Broadwater, J. and Banerjee, A., A comparison of kernel functions for intimate mixture models. In IEEE GRSS Workshop on Hyperspectral Imaging and Signal Processing: Evolution in Remote Sensing, Grenoble, France, 2009, pp. 1–4.
19. Broadwater, J., Chellappa, R., Banerjee, A. and Burlina, P., Kernel fully constrained least squares abundance estimates. In Proceedings of the IEEE International Geological and Remote Sensing Symposium, Barcelona, Spain, 2007, pp. 4041–4044.
20. Wu, X., Li, X. and Zhao, L., A kernel spatial complexity-based nonlinear unmixing method of hyperspectral imagery. In Proceedings of the Life System Modeling and Intelligent Computing, Springer, Berlin, Heidelberg, 2010, pp. 451–458.
21. Altmann, Y., Dobigeon, N. and Tourneret, J., Nonlinearity detection in hyperspectral images using a polynomial post-nonlinear mixing model. *IEEE Trans. Image Process.*, 2013, **22**(4), 1267–1276.
22. Altmann, Y., Dobigeon, N., Tourneret, J. Y. and Bermudez, J. C. M., A robust test for nonlinear mixture detection in hyperspectral images. In Proceedings of the IEEE International Conference Acoustic, Speech and Signal Processing, Vancouver, Canada, 2013, pp. 2149–2153.
23. Somers, B., Cools, K., Delalieux, S., Stuckens, J., Zande, D., Verstraeten, W. and Coppin, P., Nonlinear hyperspectral mixture analysis for tree cover estimates in orchards. *Remote Sensing Environ.*, 2009, **113**, 1183–1193.
24. Chen, J., Richard, C. and Honeine, P., Nonlinear unmixing of hyperspectral data based on a linear–mixture/nonlinear fluctuation model. *IEEE Trans. Signal Process.*, 2013, **60**(2), 480–492.
25. Eches, O., Dobigeon, N. and Tourneret, J.-Y., Enhancing hyperspectral image unmixing with spatial correlations. *IEEE Trans. Geosci. Remote Sensing*, 2011, **49**(11), 4239–4247.
26. EO1 User Guide, Version 2.3, 2003.
27. Jensen, J., *Introductory Digital Image Processing: A Remote Sensing Perspective*, Pearson, 1996, 2nd edn.
28. Winter, M., Fast autonomous spectral end-member determination in hyperspectral data. In Proceedings of the 13th International Conference on Applied Geologic Remote Sensing, Vancouver, 1999, vol. 2, pp. 337–344.
29. Plaza, A., Martínez, P., Pérez, R. and Plaza, J., A quantitative and comparative analysis of endmember extraction algorithms from hyperspectral data. *IEEE Trans. Geosci. Remote Sensing*, 2004, **42**(3), 650–663.
30. Chakravorty, S., Analysis of end-member detection and subpixel classification algorithms on hyperspectral imagery for tropical mangrove species discrimination in the Sunderbans Delta, India. *J. Appl. Remote Sensing*, 2013, **7**(1), 073523; doi:10.1117/1.JRS.7.073523.
31. Chakravorty, S. and Sinha, D. D., Analysis of multiple scattering of radiation amongst end members in a mixed pixel of hyperspectral data for identification of mangrove species in a mixed stand. *J. Indian Soc. Remote Sensing*, 2015, doi:10.1007/s12524-014-0437-x.

ACKNOWLEDGEMENTS. We thank the Department of Science and Technology, New Delhi for financial support in the form of a major research project.

Received 11 February 2016; revised accepted 30 May 2016

doi: 10.18520/cs/v111/i6/1055-1062
